

Generation of linear and nonlinear waves in numerical wave tank using CT-VOF method*

H. SAGHI¹, M. J. KETABDARI², S. BOOSHI²

(1. Department of Civil Engineering, Ferdowsi University, Mashhad, Iran;

2. Faculty of Marine Technology, Amirkabir University of Technology, Tehran, Iran)

Abstract In this paper, a two-dimensional numerical model is developed for wave simulation and propagation in a wave flume. The fluid flow is assumed to be viscous and incompressible and Navier-Stokes and continuity equations are used as governing equations. Standard k - ε model is used to model turbulent flow. The Navier-Stokes equations are discretized using staggered grids finite difference method and solved by SMAC method. Waves are generated and propagated using a piston type wave maker. An open boundary condition is used at the end of numerical flume. Some standard tests such as lid-driven cavity, constant unidirectional velocity field, shearing flow and dam-break on dry bed are performed to valid the model. To demonstrate the capability and accuracy of the present method, the results of generated waves were compared with available wave theories. Finally, clustering technique (CT) is used for mesh generation and the best condition is suggested.

Key words numerical wave tank, free surface simulation, Navier-Stokes equations, staggered grids, clustering technique, wave generation

Chinese Library Classification

2010 Mathematics Subject Classification 76T15, 80A20

1 Introduction

Numerical wave tank (NWT) is widely used on studies of offshore structures. Several researches have been focused on this topic in the past decade. Contento^[1], Grilli et al.^[2], Fochesato et al.^[3], and Ducrozet et al.^[4] considered the fluid to be inviscid to generate waves in a numerical wave tank. While Park et al.^[5], Li and Lin^[6] considered it as viscous. For wave generation and propagation in viscous fluid flow, there is a need for an accurate representation of the interface separating two immiscible fluids (air and water). Different numerical techniques such as marker and cell (MAC), height function, level set and volume of fluid (VOF) are designed for interface reconstruction. In VOF method, a fractional volume or colour function is defined to indicate the fraction of a mesh cell filled with fluid of a particular type^[7]. Troch and De Rouck^[8], Choi and Yoon^[9] and Zhao et al.^[10] used VOF method to generate waves in a numerical wave tank. In this regard, researchers used different methods for wave generation. Schaffer and Steenberg^[11], Bin and De-zhi^[12] and Li and Lin^[6] used wave maker theories for

* Received Sept. 13, 2011 / Revised Mar. 28, 2012

Corresponding author M. J. KETABDARI, Associate Professor, Ph. D., E-mail: ketabdar@aut.ac.ir

wave generation. While, Wei et al.^[13], Lara et al.^[14] and Lin and Karunarathna^[15] used mass source function of the continuity equation. Shin et al.^[16] developed a numerical model for wave generation on a continuously deforming bed. The above literature review shows that the focus in previous works is mostly on methods of wave generation and less attentions is paid on techniques of mesh generation. In this research, a numerical model was developed to generate Airy and solitary waves in a numerical wave tank using RANSE and different wave maker theories. To increase the accuracy of interface reconstruction, CT-VOF technique was used.

2 Governing equations

In this research, the fluid is considered to be Newtonian, viscous and incompressible. Therefore, 2D continuity and Navier-Stokes equations are used as:

$$\nabla \cdot V = 0, \quad (1)$$

$$\rho \left(\frac{\partial V}{\partial t} + (V \cdot \nabla)V \right) = -\nabla p + \rho g + \nabla \cdot (\mu(\nabla V + \nabla V^T)), \quad (2)$$

where t is the time, V is the velocity vector, p is the dynamic pressure, μ is the kinematic fluid viscosity, ρ is the density and g is the gravity acceleration. In the turbulent flow, the effect of turbulence can be considered using eddy viscosity models^[17]. Researchers have used different models such as k - ε and k - ω ^[18-21] to model turbulent flow. In the turbulent flow, the effect of turbulence can be considered by a variation in viscosity. In this paper, the standard two equation k - ε model is used, where one equation involves turbulence kinetic energy (k) represents the velocity scale and the other takes into account turbulent dissipation rate (ε) represents the length scale. The two-equation k - ε turbulence model to account for the effect of turbulence as follows:

$$\frac{\partial k}{\partial t} + \frac{\partial uk}{\partial x} + \frac{\partial vk}{\partial y} = \frac{\partial}{\partial x} \left(\nu_k \frac{\partial k}{\partial x} \right) + \frac{\partial}{\partial y} \left(\nu_k \frac{\partial k}{\partial y} \right) - G_S - \varepsilon, \quad (3)$$

$$\frac{\partial \varepsilon}{\partial t} + \frac{\partial u\varepsilon}{\partial x} + \frac{\partial v\varepsilon}{\partial y} = \frac{\partial}{\partial x} \left(\nu_\varepsilon \frac{\partial \varepsilon}{\partial x} \right) + \frac{\partial}{\partial y} \left(\nu_\varepsilon \frac{\partial \varepsilon}{\partial y} \right) - C_{\varepsilon 1} G_S - C_{\varepsilon 2} \frac{\varepsilon^2}{k}, \quad (4)$$

where

$$\nu = \frac{\mu}{\rho}, \quad (5)$$

$$\nu_\varepsilon = \nu + \frac{\nu_t}{\sigma_\varepsilon}, \quad (6)$$

$$G_S = \nu_t \left(2 \left(\frac{\partial u}{\partial x} \right)^2 + 2 \left(\frac{\partial v}{\partial y} \right)^2 + \left(\frac{\partial u}{\partial y} + \frac{\partial v}{\partial x} \right)^2 \right), \quad (7)$$

$$\nu_k = \nu + \frac{\nu_t}{\sigma_{k\varepsilon}}, \quad (8)$$

$$\nu_t = \frac{C_\mu k^2}{\varepsilon}, \quad (9)$$

and C_μ , $C_{\varepsilon 1}$, $C_{\varepsilon 2}$, σ_ε and σ_k are defined in Table 1.

Table 1 Coefficients for standard k - ε turbulence model

C_μ	$C_{\varepsilon 1}$	$C_{\varepsilon 2}$	σ_ε	σ_k
0.09	1.44	1.92	1.0	1.3

In this paper, volume of fluid method is used for free surface tracking. The fluid is modeled by a step function of $f(x, y, t)$ which is equal to one in points where fluid particles exist and zero elsewhere. This function is expressed as^[22-25]

$$\frac{\partial f}{\partial t} + (\nu \cdot \nabla)f = 0. \quad (10)$$

Based on this equation, f varies respect to both time and space which its spectrum can be represented as:

$$F_i(t) = \frac{1}{A_i} \int_{A_i} f_i(x, t) dx. \quad (11)$$

Combining Eqs. (10) and (11) we have

$$\frac{\partial F}{\partial t} + (\nu \cdot \nabla)F = 0, \quad (12)$$

where F has a specific value in each scalar cell as follows:

$$F = \begin{cases} 1 & \text{inside water,} \\ 0 & \text{inside air,} \\ \text{between } 0 \text{ and } 1 & \text{free surface cells.} \end{cases} \quad (13)$$

In this paper, Youngs' Volume of Fluid (Y-VOF) method is used to model free surface tracking. The interface within cell (i, j) is approximated by a straight line segment with orientation $\beta_{i,j}$ which cut the cell in such a way that the fractional fluid volume is satisfied. Four possible interface reconstructions for Y-VOF method are shown in Fig. 1.

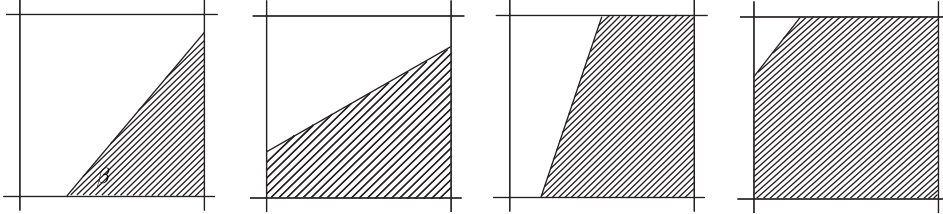


Fig. 1 Four possible interface reconstruction for Y-VOF method

To calculate $\beta_{i,j}$, normal vectors on surface are estimated as:

$$\beta_{i,j} = \tan^{-1} \left(\frac{-n_{i,j}^x}{n_{i,j}^y} \right), \quad -\pi < \beta_{i,j} < \pi, \quad (14)$$

$$n_{i,j}^x = \frac{1}{\Delta x} (F_{i+1,i+1} + 2F_{i+1,i} + F_{i+1,i-1} - F_{i-1,i+1} - 2F_{i-1,i} - F_{i-1,i-1}), \quad (15)$$

$$n_{i,j}^y = \frac{1}{\Delta x} (F_{i+1,i+1} + 2F_{i,i+1} + F_{i+1,i+1} - F_{i+1,i-1} - 2F_{i,i-1} - F_{i-1,i-1}), \quad (16)$$

where Δx and Δy are the mesh sizes in the x - and y -directions and $F_{i,j}$ is colour function. Other parameters are described similarly.

The geometry of the fluid is then used to determine the fluxes through any side on which the velocity is directed out of the cell. This method is also direct split. It means that the fluxes

in the x - and y -directions are estimated separately. In application of VOF method, colour functions in the cells of domain are updated at each time step. Then, domain is considered as a fluid with variable density and viscosity as

$$\rho_{\text{eff}} = F_{i,j}\rho_{\text{water}} + (1 - F_{i,j})\rho_{\text{air}}, \quad (17)$$

$$\mu_{\text{eff}} = F_{i,j}\mu_{\text{water}} + (1 - F_{i,j})\mu_{\text{air}}, \quad (18)$$

$$\nu_{\text{eff}} = \frac{\mu_{\text{eff}}}{\rho_{\text{eff}}}. \quad (19)$$

Now, kinematic viscosity (ν) is replaced by the effective kinematic viscosity (ν_{eff}) in Eqs. (2) and (3) as final governing equations.

3 Solution algorithm and stability criteria

In this study, the simplified marker and cell method (SMAC) is used to solve the time-dependent NSE. The governing equations are discretized on a Cartesian staggered grid system^[26]. In this method, a two-step advancement algorithm is used as

$$\frac{\hat{U} - U^n}{\Delta t} = -\text{conv}^n + \text{Diff}^n + B^n, \quad (20)$$

$$\frac{U^{n+1} - U^n}{\Delta t} = -\nabla P^{n+1}, \quad (21)$$

where U^n is the velocity field in old time level, \hat{U} is the intermediate velocity field, U^{n+1} is the new velocity field, conv^n is the convection term, Diff^n is the diffusion term and B^n is the body force term consist of gravity acceleration. The present method is explicit and first order in time, whereas the order of the space discretisation depends on the scheme used for the convective terms. As velocity field should satisfy the continuity equation, if the divergence of Eq. (21) is taken, the following Poisson's equation for the pressure is derived as:

$$\nabla^2 P^{n+1} = \frac{1}{\Delta t} \nabla \hat{U}. \quad (22)$$

The intermediate velocity field is obtained by Eq. (20). Then, the pressure distribution in the new time level is achieved using Eq. (22). Finally, the new velocity field is estimated using Eq. (21). The position of the free surface is then updated using VOF method. In this procedure, time step was selected based on two stability criteria^[27] as Courant and diffusion conditions as follows:

$$\Delta t_c = \min \left(\min \left(\frac{\Delta x_i}{|u_{i,j}|} \right), \min \left(\frac{\Delta y_j}{|v_{i,j}|} \right) \right), \quad (23)$$

$$\Delta t_v = \frac{1}{2} \left(\frac{1}{\nu_e \left(\left(\frac{1}{\Delta x_i} \right)^2 + \left(\frac{1}{\Delta y_j} \right)^2 \right)} \right). \quad (24)$$

Using the above mentioned relationships, the time step must be selected as the smallest one in the numerical simulation. One of the key problems for accurately simulation of wave propagation in a wave flume is the quality of mesh generation. Most of the researchers used uniform structured grid mesh. In this research, two different clustering techniques are used in mesh generation as shown in Fig. 2 to find their effect on accuracy of wave generation in NWT.



Fig. 2 Clustering technique in mesh generation

In local clustering, the height of meshes adjacent to the bottom and top walls and free surface (h_f) are less than those of in other places (h_{other}) so that $h_f = h_{\text{other}}/LCC$. In exponential clustering, the height of meshes is decreased from bottom and top walls towards free surface location with successive ratio as Exponential Clustering Coefficient (ECC).

4 Model validation

Before using the developed model for wave generation, its performance and accuracy must be evaluated. In this section a series of standard tests are carried out to validate the model.

4.1 Lid-driven cavity

The fluid flow is in a rectangular container which moves tangentially to itself and parallel to one of the side walls. Due to the simplicity of the cavity geometry, applying a numerical method on this flow problem in terms of coding is quite easy and straight forward. Despite its simple geometry, the driven cavity flow retains a rich fluid flow physics manifested by multiple counter rotating recirculation regions on the corners of the cavity depending on the Reynolds number (Re). The model is then run for different Re and results were compared with those of Ghia et al.^[28]. The results for $Re = 1000$ and 10000 are shown in Figs. 3 and 4. As can be seen in these figures, there are a very good agreement between the results.

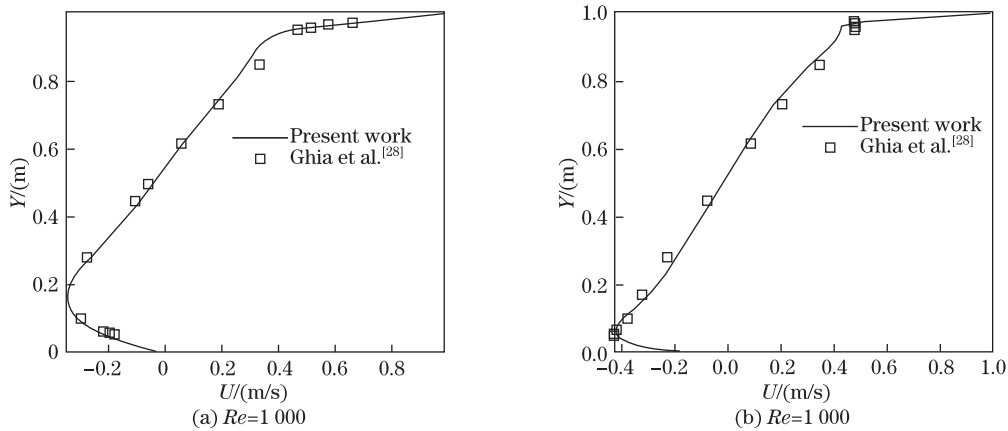


Fig. 3 Lid-driven cavity test, comparison between results of horizontal velocity of present model and those of Ghia et al.^[28]

4.2 Constant unidirectional velocity field

The simplest test involves advection of a geometric shape in the computational domain. In this test, the geometric shape should remain intact, and total amount of the fluid within the region should be conserved. The test examined here is a hollow box being translated by

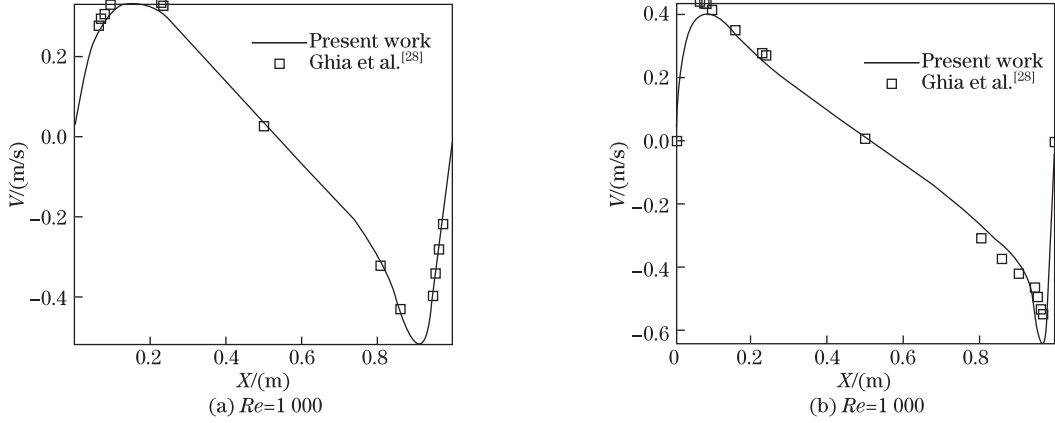


Fig. 4 Lid-driven cavity test, comparison between results of vertical velocity of present model and those of Ghia et al.^[28]

a uniform constant velocity field. This is selected to highlight the problem existing in some recent methods^[29]. The 2D Cartesian region of $1\text{ m} \times 1\text{ m}$ is composed equally sized cells. A square fluid blocks of $0.1\text{ m} \times 0.1\text{ m}$ moves with equal horizontal and vertical velocities of 1 m/s towards the top right-hand corner of the computational domain. Figure 5 shows the results. The computational time step in these calculations is 1×10^{-3} sec yields a courant number of 0.1. Results show acceptable agreement between the result of model and exact solution.

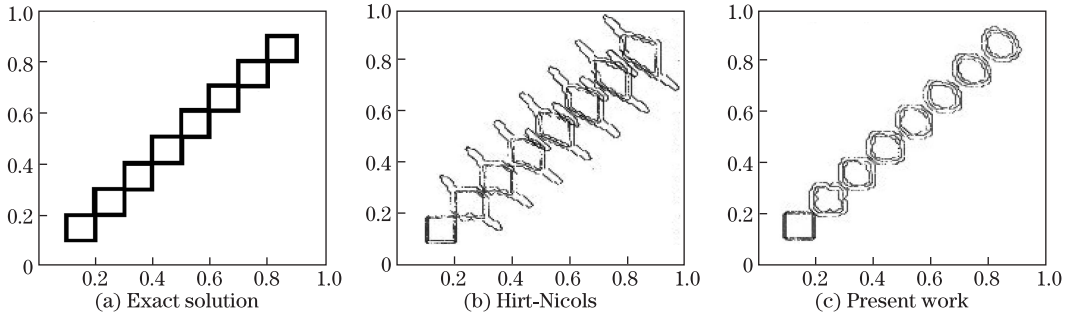


Fig. 5 Numerical results of advection test for VOF model validation

4.3 Breaking dam

Another test case used for free surface problem is the collapse of water column over a dry bed. This test is a very useful benchmark providing extreme conditions to assess the numerical stability as well as the capability of the model to treat the free surface problem. In this test, a square computational domain with a length and height of 22.8 cm is set. A water column with the width and height of 5.7 cm and 11.4 cm is considered at the left of the computational domain as shown in Fig. 6. The no-slip boundary condition is used for walls. The mesh size in the x - and y -directions are $\Delta x = \Delta y = 0.1L$. The experimental data given by Martin and Moyce^[30] are used for model validation. The results as shown in Fig. 7 prove the accuracy and capability of the model to free surface modeling.

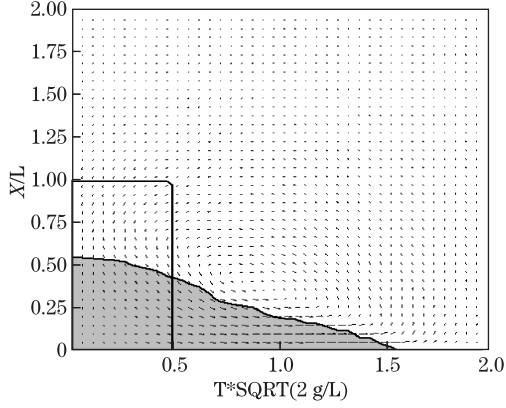


Fig. 6 Study domain of dam break modeling

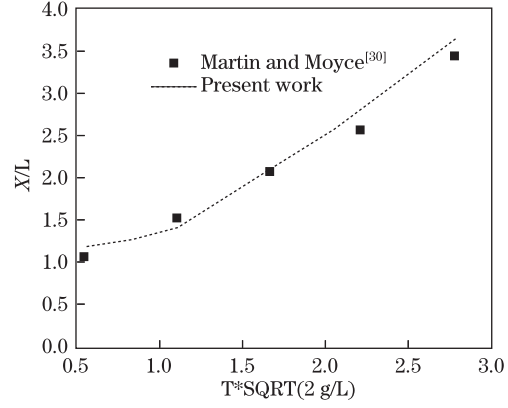


Fig. 7 Comparison between the results of model and the experimental data in dam break test from Martin and Moyce^[30]

5 Numerical wave tank

In this section, NWT is used for generation of linear and nonlinear waves represented by airy and solitary waves. The tank had a length of 18 m, width of 1m and depth of 0.9 m. A piston type wave maker was set at the left lateral boundary. At the cell boundary where the computational cell is adjacent to the solid cell, a no-slip wall boundary condition is used for velocity^[31]. In adjacent wall, adhesion is not considered. Therefore, the Neumann boundary condition is used for the color function over there.

5.1 Initial and boundary conditions

The initial condition for pressure was assumed to be hydrostatic in the domain. In the inflow boundary, the components of velocity are specified and the pressure is extrapolated from the interior of the computational domain by assuming a zero pressure gradient. The related formulas are presented in 5.2 and 5.3. For bottom boundary, zero normal velocity and horizontal no-slip conditions were considered. In the outflow boundary, the pressure is extrapolated from the interior of the computational domain by assuming a zero pressure gradient. An open boundary with velocity condition is used in the outflow boundary as follows:

$$U_{\text{OpenBoundary}} = g\eta \frac{\omega}{k}, \quad (25)$$

where ω is the wave angular frequency, k is the wave number, g is the gravity acceleration and η is the free surface elevation.

5.2 Linear wave

Herein, the small amplitude waves were generated by prescribing the inflow velocities based on the orbital motion of water particles using the linear wave theory. The relationships between piston velocity and generated Airy wave characteristics are presented as follows:

$$U_{\text{wavemaker}} = \frac{2kh + \sinh(2kh)}{2(\cosh(2kh) - 1)} \omega a \cos(\omega t), \quad (26)$$

where parameter a is the wave amplitude. Here, a wave with a length of 2.8 m and a height of 0.08 m was generated. At the first step, mesh independency is checked. So, different mesh numbers in the x and y directions are selected to generate waves in numerical model. To validate the model, the results are compared with those of linear wave maker theory. For example, the results belong to the cases with 482, 602, and 723 meshes in the x direction and 52, 62, and 78

meshes in the y direction are presented in Fig. 8. The existence of a good agreement between results is evident in this figure.

So, 602×62 meshes is adopted for the future calculations. In the next step, different clustering meshes are used to generate Airy waves. The results are shown in Figs. 9 and 10.

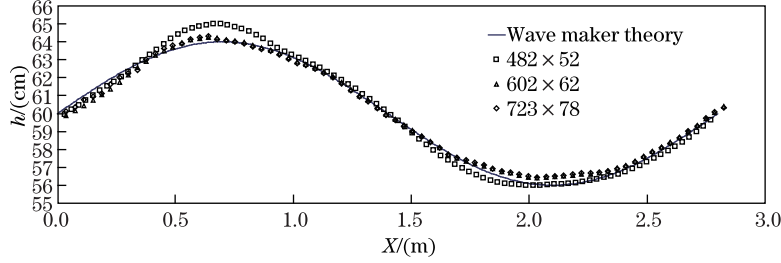


Fig. 8 Mesh independency in generation of Airy wave in NWT

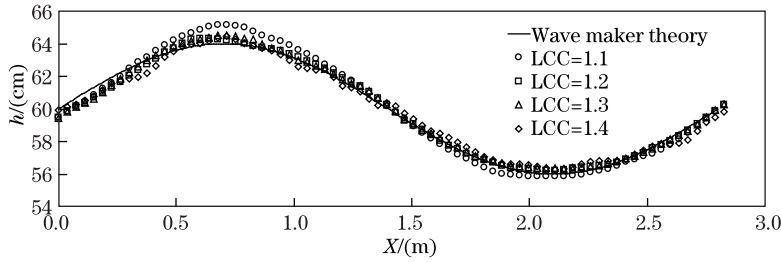


Fig. 9 Comparison of local clustering technique with different clustering coefficients (LCC) used for Airy wave generation with wave maker theory

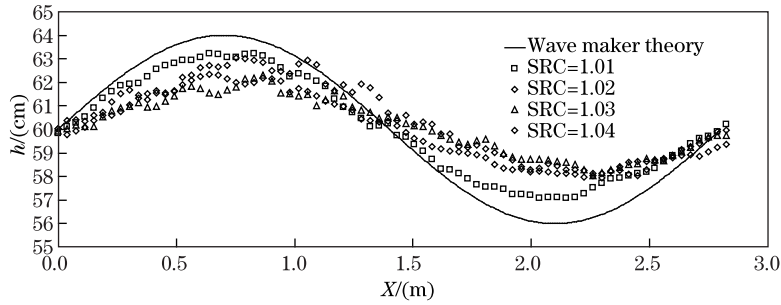


Fig. 10 Comparison of exponential clustering technique with different clustering coefficients (ECC) used for Airy wave generation with wave maker theory

To compare the results obtained using different clustering coefficient in local and exponential algorithms, two error criteria as sum square error (SSE) and sum absolute error (SAE) are calculated. The results are summarized in Table 2.

Table 2 Comparison of SSE and SAE errors of different clustering coefficient to generate Airy wave

Error	Local clustering				Exponential clustering			
	LCC=1.1	LCC=1.2	LCC=1.3	LCC=1.4	ECC=1.01	ECC=1.02	ECC=1.03	ECC=1.04
SSE	18.720 3	5.102 1	6.072 5	9.948 2	50.533 1	171.686 5	245.964 6	191.054 9
SAE	30.587 49	15.030 6	17.195 3	23.138 5	54.515 8	100.841 8	120.075 9	105.434 8

The results show that using local clustering technique using coefficient LCC=1.2 gives the most accurate results for Airy waves.

5.3 Solitary wave

In this section, developed model is used to generate solitary wave. Solitary wave is a long wave associated with quasi vertically uniform flow of horizontal velocity. Therefore, piston-type wave maker seems to be a suitable generation device for this type of wave. The usual procedure for long-wave and more specifically solitary wave generation consists of matching the paddle velocity at each position in time with the vertically averaged horizontal velocity of the wave. This can be expressed as:

$$\frac{dX}{dt} = \bar{u}(X, t), \quad (27)$$

where X is the paddle position along the x -axis and $\bar{u}(X, t)$ is the long wave depth-averaged horizontal velocity in location x and time t .

There are different laws of motion for paddle to generate solitary waves. A solitary wave is a steady solution in the wave co-moving frame travelling at the wave phase speed c (celerity). Hence, Eq. (27) can be re-written as

$$\frac{dX}{d\theta} = \frac{\bar{u}(\theta)}{c - \bar{u}(\theta)}, \quad (28)$$

where $\theta = ct - X$. $\bar{u}(\theta)$ can be obtained as^[32-33]:

$$\bar{u}(\theta) = \frac{cA \sec h^2(\beta\theta/2)}{h_0 + A \sec h^2(\beta\theta/2)}, \quad (29)$$

where A is the solitary wave amplitude, h_0 is the mean water depth, c is the phase speed and β is the outskirts decay coefficient. Integrating Eqs. (28) and (29) yields

$$X(t) = \frac{2A}{h_0\beta \tanh(\beta(ct - X(t))/2)}. \quad (30)$$

The total stroke of the paddle S can be deduced as

$$S = \frac{4A}{h_0\beta}, \quad (31)$$

The two solitary wave expressions differ in terms of the values of c and β . There are some equations such as Goring^[8], shallow water first order/KdV^[34] and Shallow water second order^[35] to model the paddle motion. In this study, the Boussinesq solitary wave equation presented by Goring is used to generate solitary waves. For c and β based on the best agreement with experimental work, the following relations are presented:

$$c = \sqrt{g(h_0 + A)}, \quad (32)$$

$$\beta = \sqrt{\frac{3A}{h_0^3}}. \quad (33)$$

Finally, paddle movement is expressed as:

$$X(t) = S_G \tanh\left(\frac{t}{\tau} - 0.5\right), \quad (34)$$

where S_G and τ are the total stroke and duration of the paddle motion respectively as

$$S_G = 4\sqrt{Ah_0/3}, \quad (35)$$

$$\tau = \frac{4}{\beta c} \left(\tanh^{-1}(0.9999) + \frac{A}{h_0} \right). \quad (36)$$

Here, a Solitary wave with a wave length of 18.0 m and a wave height of 0.06 m was generated considering mesh independency problem. For validation of the model, the results are compared with those of nonlinear wave maker theory. The results for cases with 482, 602, and 723 meshes in the x -direction and 52, 62, and 78 meshes in the y -direction in Fig. 11 show existence of a good agreement between results.

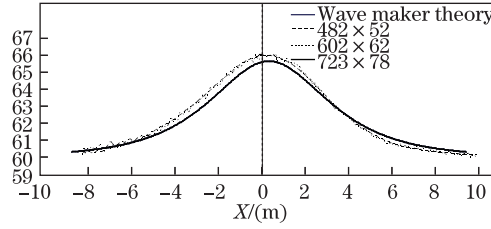


Fig. 11 Mesh independency in generation of solitary wave in NWT

In this step, different mesh types as shown in Fig.1 with 602×62 meshes and different clustering coefficients are used to generate solitary waves. Figures 12 and 13 show the results.

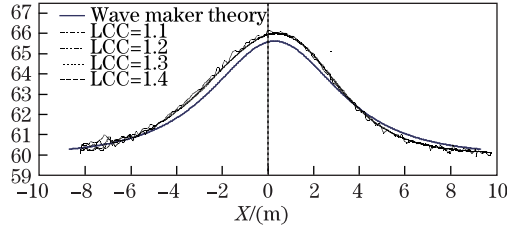


Fig. 12 Comparison of local clustering technique with different clustering coefficients (LCC) used for solitary wave generation with wave maker theory

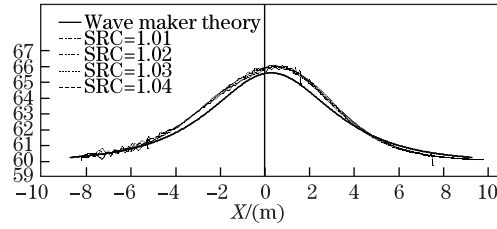


Fig. 13 Comparison of exponential clustering technique with different clustering coefficients (ECC) used for solitary wave generation with wave maker theory

To compare the results obtained using different clustering coefficients, SSE and SAE are calculated. The results are summarized in Table 3.

Table 3 Comparison of SSE and SAE errors of different clustering coefficients to generate solitary waves

Error	Local clustering				Exponential clustering			
	LCC=1.1	LCC=1.2	LCC=1.3	LCC=1.4	ECC=1.01	ECC=1.02	ECC=1.03	ECC=1.04
SSE	179.503	130.957	136.466 8	136.903 4	139.764 7	104.778 8	111.933	134.1
SAE	250.555	213.726	216.979 9	215.608 7	211.953 3	183.779	187.451	208.8

The results show that using exponential clustering using coefficient ECC=1.02 gives the most accurate results for solitary wave generation.

6 Discussion and conclusions

In this paper, a numerical wave tank is simulated to generate linear and nonlinear waves. In the develop model, The Navier-Stokes equations were used as governing equations. These equations were discretized by finite difference method in staggered grids and solved using SMAC method. To validate the model, the results are compared with those of linear and nonlinear wave maker theories. The existence of a good agreement between developed code results and theory was evident. The results also showed that using local clustering technique with clustering coefficient of 1.2 and exponential clustering technique with clustering coefficient of 1.02 gives the best results for linear and nonlinear wave generation.

References

- [1] Contento, G. Numerical wave tank computations of nonlinear motions of two-dimensional arbitrarily shaped free floating bodies. *Ocean Engineering*, **27**, 531–556 (2000)
- [2] Grilli, S. T., Vogelmann, S., and Watts, P. Development of a 3D numerical wave tank for modeling tsunami generation by underwater landslides. *Engineering Analysis With Boundary Elements*, **26**, 301–313 (2002)
- [3] Fochesato, C., Grilli, S., and Dias, F. Numerical modeling of extreme rogue waves generated by directional energy focusing. *Wave Motion*, **44**, 395–416 (2007)
- [4] Ducrozet, G., Bonnefoy, F., Le Touzé, D., and Ferrant, P. A modified high-order spectral method for wavemaker modeling in a numerical wave tank. *European Journal of Mechanics B/Fluids*, 2012 (in press)
- [5] Park, J. C., Kim, M. H., Miyata, H., and Chun, H. H. Fully nonlinear numerical wave tank (NWT) simulations and wave run-up prediction around 3-D structures. *Ocean Engineering*, **30**, 1969–1996 (2003)
- [6] Li, Y. and Lin, M. Regular and irregular wave impacts on floating body. *Ocean Engineering*, **42**, 93–101 (2012)
- [7] Rudman, M. Volume-tracking methods for interfacial flow calculations. *International Journal for Numerical Methods in Fluids*, **24**, 671–691 (1997)
- [8] Troch, P. and De Rouck, J. An active wave generating-absorbing boundary condition for VOF type numerical model. *Coastal Engineering*, **38**, 223–247 (1999)
- [9] Choi, J. W. and Yoon, S. B. Numerical simulation using momentum source wave-maker applied RANSE equation model. *Coastal Engineering*, **56**, 1043–1060 (2009)
- [10] Zhao, X. Z., Hu, C. H., and Sun, Z. C. Numerical simulation of extreme wave generation using VOF method. *Journal of Hydrodynamics*, **22**, 466–477 (2010)
- [11] Schäffer, H. A. and Steenberg, C. M. Second-order wavemaker theory for multidirectional waves. *Ocean Engineering*, **30**, 1203–1231 (2003)
- [12] Bin, T. and De-zhi, N. A simplified model for extreme-wave kinematics in deep sea. *J. Marine. Sci. Appl.*, **8**, 27–32 (2009)
- [13] Wei, G., Le, J. C., and Dai, S. Q. Surface effects on internal wave generated by a moving source in a two-layer fluid of finite depth. *Applied Mathematics and Mechanics. (English Edition)* **24**(9), 1025–1040 (2003)
- [14] Lara, J. L., Garcia, N., and Losada, I. J. RANS modelling applied to random wave interaction with submerged permeable structure. *Coastal Engineering*, **113**(3), 396–417 (2006)
- [15] Lin, P. and Karunarathna, S. A. S. Numerical study of Solitary wave interaction with porous breakwaters. *Journal of Waterway, Port, Coastal and Ocean Engineering*, **133**(5), 352–363 (2007)
- [16] Shin, S., Bae, S. Y., Kim, I. C., Kim, Y. J., and Yoo, H. K. Simulation of free surface flows using the flux-difference splitting scheme on the hybrid Cartesian/immersed boundary method. *International Journal for Numerical Methods in Fluids*, **68**(3), 360–376 (2012)
- [17] Rafei, R. *Numerical Solution of Incompressible 3D Turbulent Flow in a Spiral Channel*. M. Sc. dissertation, Amirkabir University of Technology (2004)

-
- [18] Li, C. W. and Zang, Y. F. Simulation of free surface recirculating flows in semi- enclosed water bodies by a k - w model. *Applied Mathematical Modeling*, **22**, 153–164 (1998)
- [19] Gao, H., Gu, H. Y., and Guo, L. J. Numerical study of stratified oil-water two-phase turbulent flow in a horizontal tube. *Int J Heat Mass Transfer*, **46**, 749–754 (2003)
- [20] Ren, B. and Wang, Y. Numerical simulation of random wave slamming on structures in the splash zone. *Ocean Engineering*, **31**, 547–560 (2004)
- [21] Shen, Y. M., Ng, C. O., and Zheng, Y. H. Simulation of wave propagation over a submerged bar using the VOF method with a two-equation k - ε turbulence modeling. *Ocean Engineering*, **31**, 87–95 (2004)
- [22] Mirbagheri, S. M. H., Dadashzadeh, M., Serajzadeh, S., Taheri, A. K., and Davami, P. Modeling the effect of mould wall roughness on the melt flow simulation in casting process. *Applied Mathematical Modeling*, **28**, 933–956 (2004)
- [23] Geuyffier, D., Li, J., Nadim, A., Scardovelli, R., and Zaleski, S. Volume-of-fluid interface tracking with smoothed surface stress methods for three-dimensional flows. *Journal of Computational Physics*, **152**, 423–456 (1999)
- [24] Harvie, D. J. E. and Fletcher, D. F. A new volume of fluid advection algorithm: the defined donating region scheme. *International Journal for Numerical Methods in Fluids*, **35**, 151–172 (2001)
- [25] Ketabdari, M. J., Nobari, M. R. H., and Moradi larmaei, M. Simulation of waves group propagation and breaking in coastal zone using a Navier-Stokes solver with an improved VOF free surface treatment. *Applied Ocean Research*, **30**, 130–43 (2008)
- [26] Hur, D. S. and Mizutani, M. Numerical estimation of the wave forces acting on a three-dimensional body on submerged breakwater. *Coast. Eng.*, **47**, 329–345 (2003)
- [27] Duff, E. S. Fluid Flow aAspects of Solidification Modeling, Simulation of Low Pressure Die Casting, *Ph. D dissertation*, University of Queensland (1999)
- [28] Ghia, U., Ghia, K. N., and Shin, C. T. High- Re solutions for incompressible flow using the Navier-Stokes equations and a multigrid method. *Journal of Computational Physics*, **48**, 387–411 (1982)
- [29] Scardovelli, R. and Zaleski, S. Interface reconstruction with least-square fit and split Eulerian-Lagrangian advection. *International Journal of Numerical Methods in Fluids*, **41**, 251–274 (2003)
- [30] Martin, J. C. and Moyce, W. J. An experimental study of the collapse of liquid columns on a rigid horizontal plane. *Philosophical Transaction of the Royal Society of London*, **244**, 312–324 (1982)
- [31] Shen, Y. M., Ng, C. O., and Zheng, Y. H. Simulation of wave propagation over a submerged bar using the VOF method with a two-equation k - ε turbulence modeling. *Ocean Eng.*, **31**, 87–95 (2004)
- [32] Boussinesq, M. J. Théorie de l'intumescence liquide, appelée onde solitaire ou de translation. se propageant dans un canal rectangulaire, *C.-R. Acad. Sci. Paris*, **72**, 755–59 (1871)
- [33] Rayleigh, L. On waves. *Phil. Mag.*, **1**, 257–279 (1876)
- [34] Clamond, D. and Germain, J. P. Interaction between a Stokes wave packet and a solitary wave. *Eur. J. Mech. B/Fluids*, **18**, 67–91 (1999)
- [35] Temperville, A. Contribution à l'étude des Ondes de Gravité en Eau Peu Profonde, Thèse d'Etat, Université Joseph Fourier (1985)